Supporting Information

Fu et al. 10.1073/pnas.1717695114

SI Text

Design and Fabrication of Syringe-Injectable Electronics. The scalable highly multiplexed mesh electronics for chronic brain activity mapping used a fabrication procedure similar to our recent reports (31–35). Key steps involved in the fabrication of syringe-injectable mesh electronics are overviewed in Fig. S1, with the key mesh parameters as follows: total mesh width, $W = 2$ mm; longitudinal SU-8 polymer element width, $w_1 = 20$ μm; transverse SU-8 element width, $w_2 = 20$ μm; angle between longitudinal and transverse SU-8 elements, $\alpha = 45°$; longitudinal spacing (pitch between transverse elements), $L_1 = 333$ μm; transverse spacing (pitch between longitudinal elements), $L_2 = 62.5$ μm for 32-/64-/128-channel (Figs. 1*B* and 2 *B* and *C*) mesh electronics designs; and metal interconnect line width, $w_m = 2$ μm for 32-/64-/128-channel (Figs. 1*B* and 2 *B* and *C*) mesh electronics designs. The number of recording channels on each longitudinal element $N_{each} = 1$, 2, and 4 for mesh electronics designs with total number of recording channels $n = 32$, 64, and 128, respectively. The bending stiffness calculation for the 16-channel mesh electronics probe was based on mesh design parameters reported previously (33). The key fabrication steps (Fig. S1) are as follows: (*i*) A sacrificial layer of Ni with a thickness of 100 nm was thermally evaporated (Sharon Vacuum) onto a 3-inch Si wafer (n-type 0.005 Ω·cm, 600-nm thermal oxide; Nova Electronic Materials), which was precleaned with oxygen plasma (100 W, 2 min). (*ii*) Negative photoresist SU-8 (SU-8 2000.5; MicroChem Corp.) was spin-coated on the Si wafer to a thickness of 400 nm, prebaked sequentially at 65 °C for 1 min and 95 °C for 4 min, and then patterned by PL with a mask aligner (ABM mask aligner). After PL exposure, the sample was post-baked sequentially at 65 °C for 3 min and 95 °C for 3 min. (*iii*) The SU-8 photoresist was then developed (SU-8 Developer; MicroChem Corp.) for 2 min, rinsed with isopropanol, dried in a N_2 flow, and hard-baked at 180 °C for 1 h. (*iv*) The wafer was then cleaned with oxygen plasma (50 W, 1 min), spin-coated with MCC Primer 80/20 and LOR 3A lift-off resist (MicroChem Corp.), and baked at 180 °C for 5 min, followed by spin-coating Shipley 1805 positive photoresist (Microposit; The Dow Chemical Company), which was then baked at 115 °C for 5 min. The positive photoresist was patterned by PL and developed (MF-CD-26, Microposit; The Dow Chemical Company) for 90 s. (*v*) A 1.5-nm-thick Cr layer and a 100-nm-thick Au layer were sequentially deposited by electron beam evaporation (Denton Vacuum), followed by a lift-off step (Remover PG; MicroChem Corp.) to make the Au interconnect lines. (*vi*) Steps *iv* and *v* were repeated for PL patterning and deposition of the Pt electrodes (Cr: 1.5 nm, Pt: 50 nm). The diameter of Pt sensing electrodes was 20 μm. (*vii*) Steps *ii* and *iii* were repeated for PL patterning of the top SU-8 layer, which served as the top encapsulating/insulating layer of the metal interconnect lines. The final hard-bake temperature of the top SU-8 layer was set at 190 °C (10 °C higher than that used for lower-layer hard-bake) to interdiffuse and cross-link the bottom and top SU-8 layers, thus yielding monolithic encapsulation. (*viii*) Subsequently, the Si wafer was cleaned with oxygen plasma (50 W, 1 min) and then transferred to a Ni etchant solution comprising 40% $FeCl_3$:39% HCl:H_2O = 1:1:20 to remove the sacrificial Ni layer and release the mesh electronics from the Si substrate. Released mesh electronics were rinsed with DI water and transferred to an aqueous solution of 1× PBS solution (HyClone PBS; Thermo Fisher Scientific Inc.) before use.

Mechanical Simulations.

Effective bending stiffness values of mesh electronics. We estimate the bending stiffness of the mesh electronics with different structures by finite element software ABAQUS as described previously (31). A unit cell similar to figure 1d in ref. 31 was used for the simulation, where the mesh electronics were modeled with shell elements: A homogeneous single shell section with 800-nm-thick SU-8 was assigned to the transverse elements; a composite section with three layers of 400-nm-thick SU-8, 100-nm-thick gold, and another 400-nm-thick SU-8 was assigned to the longitudinal elements. Both SU-8 and gold are modeled as linear elastic materials, with Young's moduli of 2 and 79 GPa, respectively (31). To calculate the longitudinal and transverse bending stiffness values, a fixed boundary condition was set at one of the ends parallel to the bending direction, and a small vertical displacement, d, was added at the other end. The external work, W, to bend the device was calculated. We defined the effective bending stiffness of the device as the stiffness required of a homogenous beam to achieve the same external work W under the displacement d. Therefore, the effective bending stiffness per width of the mesh electronics can be estimated as (31, 54)

$$D_{mesh} = \frac{2Wl^3}{3d^2b}, \quad \textbf{[S1]}$$

with b the width of the unit cell parallel to the bending direction, and l the thickness of the unit cell perpendicular to the bending direction.

Effective bending stiffness values of implantable probes. The effective bending stiffness per width of planar polyimide probe, $D_{polyimide}$, can be estimated as (54)

$$D_{polyimide} = E_{polyimide}\frac{h^3_{polyimide}}{12}, \quad \textbf{[S2]}$$

where $E_{polyimide} = 2$ GPa to 2.73 GPa and $h_{polyimide} = 10$ μm to 20 μm are the Young's modulus and the thickness of planar polyimide probe, respectively (39). This calculation gives $D_{polyimide} = 0.16$ to 1.3×10^4 nN·m.

The effective bending stiffness per diameter of a microwire probe, $D_{microwire}$, can be estimated as (54)

$$D_{microwire} = E_{microwire}\frac{\pi d^3_{microwire}}{64}, \quad \textbf{[S3]}$$

where $E_{microwire} = 200$ GPa to 400 GPa and $d_{microwire} = 20$ μm to 40 μm are the typical Young's modulus and diameters, respectively, for commonly used microwire probes (18, 46). This calculation gives $D_{microwire} = 0.79$ to 9.4×10^5 nN·m.

The effective bending stiffness per width of standard silicon probes, $D_{silicon}$, can be estimated as (55)

$$D_{silicon} = E_{silicon}\frac{h^3_{silicon}}{12}, \quad \textbf{[S4]}$$

where $E_{silicon} = 165$ GPa and $h_{silicon} = 15$ μm are the Young's modulus of silicon and thickness of the probe, respectively (40). This calculation gives $D_{silicon} = 4.6 \times 10^5$ nN·m.

Effective bending stiffness value of brain tissue. The effective bending stiffness per width of brain tissue, D_{brain}, can be estimated as (54)

$$D_{\text{brain}} = E_{\text{brain}} \frac{h_{\text{brain}}^3}{12}, \quad \textbf{[S5]}$$

where $E_{\text{brain}} = 1$ kPa [the median of range of 0.1 kPa to 16 kPa, Young's modulus values reported for different regions and species of brain tissue (55)], and $h_{\text{brain}} = 20$ μm to 100 μm (range of thickness of typical brain probes and single-layer brain slices). This calculation gives D_{brain} ranges from 10^{-4} nN·m to 10^{-1} nN·m.

Mesh Electronics Imaging. Wide-field images with bright-field illumination were recorded using an Olympus BX51 microscope (Olympus). Wide-field images shown in Fig. 2*B* were acquired under 5× magnification and stitched to cover the entire mesh with *ca*. 50 smaller images, each with a field of view of 1.35 mm × 1.70 mm. DIC and confocal fluorescence microscopy images were recorded using a Zeiss LSM 880 confocal microscope (Carl Zeiss Microscopy). The DIC image shown in Fig. 3*B* was acquired under 10× magnification using a 4 × 4 Tile Scan mode. Confocal images were acquired under 10× magnification using a 561-nm-wavelength laser to excite mesh electronics labeled with rhodamine-6G fluorescent dye with a 1-AU pinhole, which yields an optical section thickness of *ca*. 3 μm. A 4 × 4 Tile Scan mode was used for the acquisition of Fig. 3*C*. Each of the tile component of both confocal and DIC images has a field of view of 850 μm × 850 μm.

Electrical Characterization. Impedance measurements between adjacent 2-μm-wide Au interconnects on the same longitudinal element of the 128-channel mesh design (with an edge-to-edge distance of 2 μm) were carried out with a ∼4-mm portion of the SU-8 passivated Au interconnects immersed in 1× PBS, which approximates the in vivo recording environment, using an Agilent B1500A semiconductor device parameter analyzer (Agilent Technologies Inc.) with B1520A-FG multifrequency capacitance measurement unit (Agilent Technologies Inc.). Similarly, the impedances of Pt microelectrodes (20 μm in diameter) at the saline interface were obtained by immersing the electrodes in 1× PBS and performing the measurements using the same equipment and measurement conditions.

Vertebrate Animal Subjects. Adult (25 g to 35 g) male C57BL/6J mice (Jackson Laboratory) were the vertebrate animal subjects used in this study. Exclusion criteria were preestablished: Animals with failed surgery or substantial acute implantation damage (>100 μL of initial liquid injection volume) were discarded from further chronic recordings. Randomization or blinding study was not applicable to this study. All procedures performed on the mice were approved by the Animal Care and Use Committee of Harvard University. The animal care and use programs at Harvard University meet the requirements of the Federal Law (89-544 and 91-579) and NIH regulations and are also accredited by AAALAC. Animals were group-housed on a 12 h:12 h light:dark cycle at Harvard's Biology Research Infrastructure and fed with food and water ad libitum as appropriate.

In Vivo Mouse Survival Surgery.

Stereotaxic injection of mesh electronics in mouse brain. In vivo injections of multiple mesh electronics into the brains of live mice were performed using a controlled stereotaxic injection method described previously (32, 33). First, all metal tools in direct contact with the surgical subject were autoclaved for 1 h before use, and all plastic tools in direct contact with the surgical subjects were sterilized with 70% ethanol and rinsed with sterile DI water and sterile 1× PBS before use. Before injection, the mesh electronics were sterilized with 70% ethanol followed by rinsing in sterile DI water and transfer to sterile 1× PBS.

C57BL/6J mice were anesthetized by i.p. injection of a mixture of 75 mg/kg of ketamine (Patterson Veterinary Supply Inc.) and 1 mg/kg dexdomitor (Orion Corporation). The degree of anesthesia was verified via the toe pinch method before the surgery started. To maintain the body temperature and prevent hypothermia of the surgical subject, a homeothermic blanket (Harvard Apparatus) was set to 37 °C and placed underneath the anesthetized mouse, which was placed in the stereotaxic frame (Lab Standard Stereotaxic Instrument; Stoelting Co.) equipped with two ear bars and one nose clamp that fixed the mouse head in position. Puralube ocular lubricant (Dechra Pharmaceuticals) was applied on both eyes of the mouse to moisturize the eye surface throughout the surgery. Hair removal lotion (Nair; Church & Dwight) was used for depilation of the mouse head, and iodophor was applied to sterilize the depilated scalp skin. A 1-mm longitudinal incision along the sagittal sinus was made in the scalp with a sterile scalpel, and the scalp skin was resected using surgical scissors to expose a 6 mm × 8 mm (mediolateral × anteroposterior) portion of the skull. METABOND enamel etchant gel (Parkell Inc.) was applied over the exposed cranial bone to prepare the surface for mounting the electronics on the mouse skull later.

One-millimeter-diameter burr holes were drilled using a dental drill (Micromotor with On/Off Pedal 110/220; Grobet USA) with the number and positions defined by specific experiment and the targeted stereotaxic coordinates (see below), respectively. After each of the holes was drilled for specific mesh electronics injection, the dura was carefully incised and resected using a 27-gauge needle (PrecisionGlide; Becton Dickinson and Company). Then an additional burr hole for a grounding screw was drilled away from those prepared for the mesh injections to avoid electrical and physical interference. After dura resection, a sterilized 0-80 set screw (18-8 Stainless Steel Cup Point Set Screw; outer diameter, 0.060" or 1.52 mm; groove diameter, 0.045" or 1.14 mm; length, 3/16" or 4.76 mm; McMaster-Carr Supply Company) was screwed into this hole to a depth of 500 μm to serve as the grounding and reference electrode. The stereotaxic coordinates of injections of each mesh electronics probe for imaging and activity recording presented in this work were as follows (56):

i) For meshes 1 and 2 (Figs. 4 and 5), the initial needle/mesh tip coordinates are anteroposterior, 1.34 mm; mediolateral, ±1.50 mm (± correspond to right/left hemisphere, respectively); and dorsoventral, 1.00 mm. After controlled injection, the electrodes span from 0.90 mm to 0 mm dorsoventral to cover the entire primary motor cortex (the bottom-most electrode is 0.10 mm from the tip of the needle; the same holds hereafter).

ii) For meshes 3 and 4 (Figs. 4 and 5), the initial needle/mesh tip coordinates are anteroposterior, −1.70 mm; mediolateral, ±2.00 mm; and dorsoventral, 2.05 mm. After controlled injection, the electrodes span from 1.95 mm to 1.05 mm dorsoventral to cover both hippocampal CA1 and CA3 fields.

iii) For the meshes in Fig. 6, the initial needle/mesh tip coordinates are anteroposterior: −1.70 mm; mediolateral, 2.00 mm; and dorsoventral, 2.05 mm. After controlled injection, the electrodes span from 1.95 mm to 0.10 mm dorsoventral to cover hippocampal CA1 and CA3 fields and primary somatosensory cortex.

The dura was removed from the burr hole drilled for mesh electronics injection, and sterile 1× PBS was swabbed on the surface of the brain to keep it moist throughout the surgery. The mesh electronics were injected into the desired brain region

using a controlled injection method (32, 33). In brief, the mesh electronics were loaded into a glass capillary needle with ID of 400 μm and outer diameter (OD) of 650 μm (Drummond Scientific Co.). The glass capillary needle loaded with mesh electronics was mounted onto the stereotaxic stage through a micropipette holder (Q series holder; Harvard Apparatus), which was connected to a 5-mL syringe (Becton Dickinson and Company) through a polyethylene Intramedic catheter tubing (ID 1.19 mm, OD 1.70 mm). Controlled injection was achieved by balancing the volumetric flow rate (typically 20 mL/h to 50 mL/h), which was controlled by a syringe pump (PHD 2000; Harvard Apparatus), and the needle withdrawal speed (typically 0.2 mm/s to 0.5 mm/s), which was controlled by a motorized linear translation stage (860A motorizer and 460A linear stage; Newport Corporation). Using the controlled injection method with field of view visualization through an eyepiece camera (DCC1240C; Thorlabs Inc.), mesh electronics were delivered to targeted brain regions with elongated morphology along the injection direction with ~20-μm precision. For successful long-term recordings, the total injection volume for each injection was usually between 10 and 100 μL. An unexpected large injection volume (>100 μL) could result in brain edema or failure of recovery from acute surgical damage, leading to expulsion of the subject from the study.

Electrical connection of mesh electronics for chronic recordings from awake and restrained mice. After the injection of each of the four 32-channel mesh electronics probes into the specified region of a mouse brain, the stereotaxic stage was moved to reposition the glass capillary needle over one of four vertically and horizontally stacked 33-channel FFCs (Molex Incorporated), and then the remaining mesh electronics were fully expelled from the needle and unfolded onto the FFC to expose the I/O connection pads. High-yield bonding of mesh electronics I/O pads to the FFC was carried out using our reported conductive ink printing method (32, 33). In brief, the print head loaded with carbon nanotube solution (Stock No. P093099-11; Tubes@Rice) was driven by a motorized micromanipulator (MP-285/M; Sutter Instrument) through a user-written LabVIEW program to print conductive ink automatically and connect each mesh I/O pad to each of the FFC lines to enable independently addressable sensor elements. Failure of mesh I/O unfolding could lead to potential low-yield electrical connection to the FFC interface cable. All printed conductive lines were passivated by METABOND dental cement (Parkell Inc.), and then all of the FFCs with mesh electronics bonded were vertically stacked and cemented to the mouse skull with METABOND dental cement. The FFCs were folded to reduce their sizes on the mouse skull. The total mass of all four FFCs for four 32-channel mesh electronics probes recordings is typically 0.5 g to 0.6 g.

Electrical connection of mesh electronics for chronic recordings from freely behaving mice. After the injection of a mesh electronics probe into the specified mouse brain region, the stereotaxic stage was manually moved to reposition the glass capillary needle to a 32-channel FFC (PREMO-FLEX; Molex Incorporated), which was trimmed to reduce the total length to *ca*. 1 cm, and then the remaining mesh electronics were fully expelled from the needle and unfolded onto the FFC. Conductive ink printing was used to bond the mesh electronics I/O pads to the FFC cable. The FFC was then inserted into a ZIF connector (Molex Incorporated) mounted on one side of a custom-designed PCB with a thickness of 1/32 inch (Advanced Circuits Inc.); the other side of the PCB had an Omnetics male connector (A79024-001; Omnetics Connector Corp.) with through-hole connections to the ZIF connector. The 0-80 grounding screw was electrically connected to one of the two predefined grounding/reference pads on the PCB using silver conductive epoxy (MG Chemicals). All printed conductive lines were protected by METABOND dental cement, before the entire packaged FFC and PCB were cemented to the mouse skull.

Postoperative care. After surgery was complete, antibiotic ointment (WATER-JEL Technologies LLC) was applied copiously around the wound, and the mouse was returned to the cage equipped with a 37 °C heating pad and its activity monitored every hour until fully recovered from anesthesia (i.e., exhibiting sternal recumbency and purposeful movement). Buprenex (Buprenorphine; Patterson Veterinary Supply Inc) analgesia was given intraperitoneally at a dose of 0.05 mg/kg body weight every 12 h for up to 48 h postsurgery.

Micro-CT. One mouse injected with four mesh electronics probes with stereotaxic coordinates specified above (Fig. 4, meshes 1 through 4), where the mesh I/O pads of each probe were bonded to one of four FFCs affixed to the mouse skull as described above, was killed via i.p. injection of Euthasol at a dose of 270 mg/kg body weight and decapitated. The decapitated mouse head was imaged using an HMXST Micro-CT X-ray scanning system with a standard horizontal imaging axis cabinet (model HMXST225; Nikon Metrology, Inc.). Imaging parameters were set as 95 kV and 93 μA for scanning the decapitated mouse head. Before scanning, shading correction and flux normalization were applied to adjust the X-ray detector. The CT Pro-3D software (ver. 2.2; Nikon-Metris) was used to calibrate centers of rotation for micro-CT sinograms and to reconstruct all 2D images. VGStudio MAX software (ver. 2.2; Volume Graphics GMbh) was used for 3D rendering and analysis of the reconstructed images.

In Vivo Chronic Brain Recording in Mice.

Chronic brain recording from awake and restrained mice. Mice with four implanted mesh electronics and FFC connectors were recorded chronically on a biweekly basis, starting from day 14 postinjection and surgery. Mice were restrained in a Tail-veiner restrainer (Braintree Scientific LLC.) while its head-mounted FFC was connected to four Intan RHD 2132 amplifier evaluation systems (Intan Technologies LLC.) through four homemade PCBs. The 0-80 set screw was used as a reference. Electrophysiological recording was made with a 20-kHz sampling rate and a 60-Hz notch filter, while the electrical impedance at 1 kHz of each recording electrode was also measured by the same Intan system.

Chronic brain recording of freely behaving mice. Mice with Omnetics connectors were recorded chronically on a biweekly basis when they were freely roaming in the cage. For recording, an Intan preamplifier chip (RHD2132 32-Channel Amplifier Board; Intan Technologies LLC) with preinstalled female Omnetics connector was connected directly to the male Omnetics connector on the PCB cemented to the mouse skull during surgery, and the mouse was allowed to roam in a cage environment. Electrophysiological recordings were made using the same Intan evaluation system with a 20-kHz sampling rate and a 60-Hz notch filter, and were synchronized with video recording of the mouse's motion inside the cage using a digital camera.

Analysis of electrophysiological recording data. The electrophysiological recording data were analyzed offline. In brief, raw recording data were filtered using noncausal Butterworth band-pass filters (filtfilt function in Matlab) in the 250- to 6,000-Hz frequency range to extract single-unit spikes (33), and in the 0.1- to 150-Hz range to extract LFP (33). The correlation coefficient maps of LFPs and single-unit spike recording traces shown in Figs. S2*B* and S4*C* were calculated based on the standard Pearson product-moment correlation coefficient for time series. Namely, for two spike traces, $Y_1(t)$ and $Y_2(t)$, the correlation coefficient between them is calculated as

$$\mathrm{Corr}(Y_1, Y_2) = \frac{\int_{T_1}^{T_2} \left(Y_1(t) - \bar{Y}_1\right)\left(Y_2(t) - \bar{Y}_2\right) dt}{\sqrt{\int_{T_1}^{T_2} \left(Y_1(t) - \bar{Y}_1\right)^2 \left(Y_2(t) - \bar{Y}_2\right)^2 dt}}, \quad \textbf{[S6]}$$

where T_1 and T_2 indicate the starting and ending time of the recording traces (in Figs. S2*B* and *S4C*, the time window is 2 s), and $\bar{Y}_i = \int_{T_1}^{T_2} Y_1(t)dt/(T_2 - T_1)$ $(i = 1, 2)$ represents the averaged value of $Y_i(t)$ over the time period between T_1 and T_2.

Single-unit spike sorting was performed by amplitude thresholding of the filtered traces, where the threshold was automatically determined based on the median of the background noise according to the improved noise estimation method (57). The average firing rate of each recording channel (Figs. 5*C* and 7*D*) was obtained by dividing the total number of recorded spikes by the total recording time. The average spike amplitude for each recording channel (Fig. 5*B*) was defined as the average peak-to-peak amplitude of all recorded spikes by that channel. The noise level for each recording channel (Fig. 5*B*) was estimated based on the median, instead of the SD, of the recording trace to minimize the influence of relatively high amplitude firing events (57). Specifically, the noise level for each recording channel was defined as the median of the absolute values of recorded traces divided by 0.6745, which provides reasonable approximation of 1 SD of the noise distribution excluding firing events according to a previous publication (57). The SNR for each recording channel (Fig. 5*B*) was then obtained by dividing the average spike amplitude by the corresponding noise estimation. All sorted spikes were then clustered to determine the number of recorded single neurons, using the WaveClus software that employs unsupervised superparamagnetic clustering (57). Spikes assigned to the same cluster were coded with the same color (Figs. 6 and 7*E*). Consistent with the correlation coefficient analyses above, all of the spike-sorting, average firing rate, and average amplitude analyses were based on the recording traces shown in Fig. 5*A* and Fig. S2*A* (2-s time window) for analyses of the simultaneous 128-channel recordings (Figs. 5 *B* and *C* and 6), and recording traces shown in Fig. 7*C* and Fig. S4 *A* and *B* (2-s time window) for analyses of the freely behaving mouse recordings (Fig. 7 *D* and *E*).

Chronic Immunohistochemistry.

Histology sample preparation. Mice with implanted highly multiplexed mesh electronics probes at postinjection times of 6 wk were anesthetized with ketamine and dexdomitor, and then were transcardially perfused with 40 mL of 1× PBS and 40 mL of 4% formaldehyde (Sigma-Aldrich Corp.), followed by decapitation. The scalp skin was removed, and the exposed skull was ground for 10 min to 20 min at 10,000 rpm using a high-speed rotary tool (Dremel). The brain was resected from the cranium and placed in 4% formaldehyde for 24 h, and then transferred to 1× PBS for another 24 h at 4 °C to remove remaining formaldehyde. The brain was transferred to incrementally increasing sucrose solutions (10 to 40%) (Sigma-Aldrich Corp.) at 4 °C to cryoprotect the tissue, transferred to cryo-OCT compound (Tissue-Tek O.C.T. Compound; VWR), and then frozen at −80 °C. The frozen sample was then sectioned into 10-μm-thick horizontal slices using Leica CM1950 cryosectioning instrument (Leica Microsystems).

Immunohistochemical staining and microscopic imaging. The brain tissue sections were rinsed three times in 1× PBS and blocked in a solution consisting of 0.3% Triton X-100 (Life Technologies) and 5% goat serum (Life Technologies) in 1× PBS for 1 h at room temperature. Slices were then incubated with the primary antibodies, rabbit anti-NeuN (1:200 dilution; Abcam), mouse anti-Neurofilament (1:400 dilution; Abcam), and rat anti-GFAP (1:500 dilution; Thermo Fisher Scientific Inc.), containing 0.3% Triton X-100 and 3% goat serum, overnight at 4 °C. NeuN is a neuron-specific nuclear protein, and stains the neural somas. Neurofilament antibody recognizes neurofilaments, intermediate filaments with a diameter of 10 nm particularly abundant in axons. GFAP is glial fibrillary acidic protein, and stains astrocytes. After incubation, slices were rinsed nine times for a total of 40 min with 1× PBS, before they were incubated with the secondary antibodies, Alexa Fluor 488 goat anti-rabbit (1:200 dilution; Abcam), Alexa Fluor 568 goat anti-mouse (1:200 dilution; Abcam), or Alexa Fluor 647 goat anti-rat (1:200 dilution; Abcam), for 1 h at room temperature; the specific choices of secondary antibodies were made based on primary antibodies used to stain a given slice. Slices were rinsed nine times for a total of 30 min after incubation with secondary antibodies, before they were mounted on glass slides with coverslips using ProLong Gold Antifade Mountant (Life Technologies). The slides remained in the dark at room temperature for at least 24 h before microscopic imaging.

Confocal fluorescence imaging of the samples was acquired on a Zeiss LSM 880 confocal microscope (Carl Zeiss Microscopy GmbH). Confocal images were acquired using 488-, 561-, and 633-nm lasers as the excitation sources for Alexa Fluor 488, Alexa Fluor 568, and Alexa Fluor 647, respectively. The mesh electronics elements in each slice were imaged with DIC on the same microscope, and positions were extracted from DIC images and assigned false blue color using a custom-written MATLAB program. The program enables manual selection of the mesh electronics boundary based on contrast of mesh ribbons in the DIC image and conversion of the extracted image to binary format, with the enclosed regions assigned with values of 1 and unselected regions assigned with values of 0. The extracted images were then merged with corresponding confocal images of the same field of view using ImageJ software for composite images shown in Fig. S3*A*. ImageJ software was used for subsequent image analysis. Fluorescence intensities of Neurofilament, NeuN, and GFAP shown in Fig. S3*B* were based on the analysis of zoomed-out images of those shown in Fig. S3*A* with a field of view of 1.2 mm × 1.2 mm, and were shown with false red, green, and cyan colors, respectively, in the composite images. The fluorescence intensities were normalized (value = 1.0, gray dashed horizontal lines) against the background values 500 μm away from the probe interface for each sample.

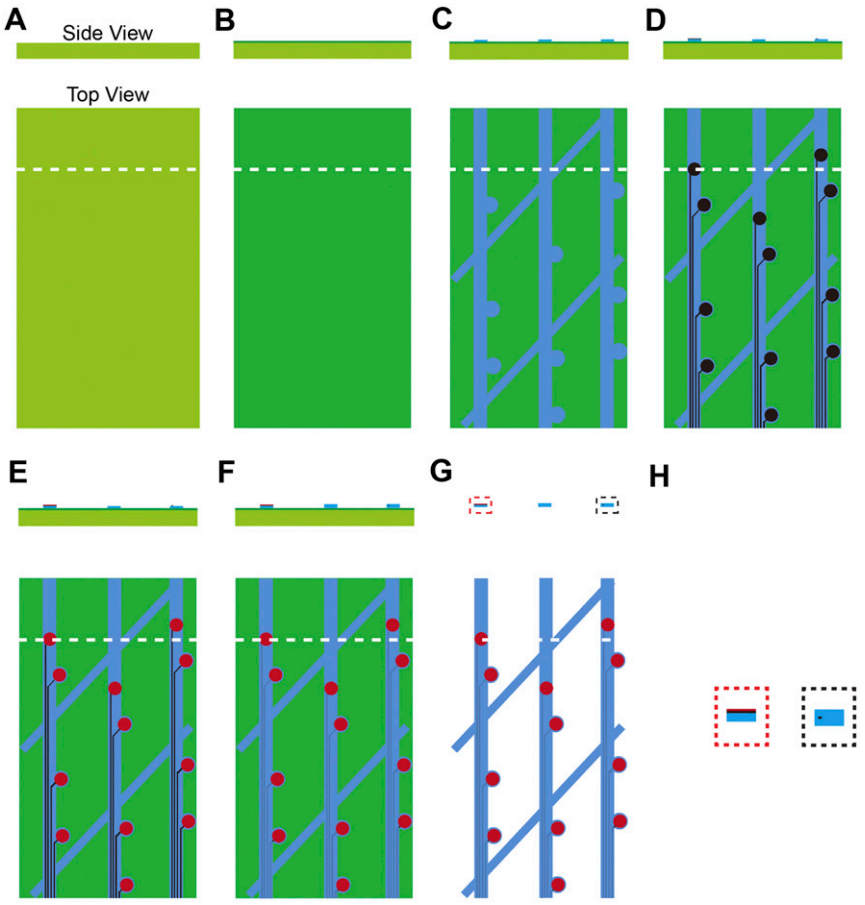

Fig. S1. Schematic steps of mesh electronics fabrication. Components include silicon wafer (light green), nickel relief layer (dark green), SU-8 mesh polymer elements (blue), Au interconnects (black), and exposed Pt electrodes (red). (*A*–*G*) For each step, both top and side views are shown, where the side view corresponds to a cross-section taken at the position indicated by the white horizontal dashed line in the top-view images. (*H*) Zoomed-in views of regions highlighted by red (exposed Pt electrodes) and black dashed boxes (fully passivated interconnects) in *G*.

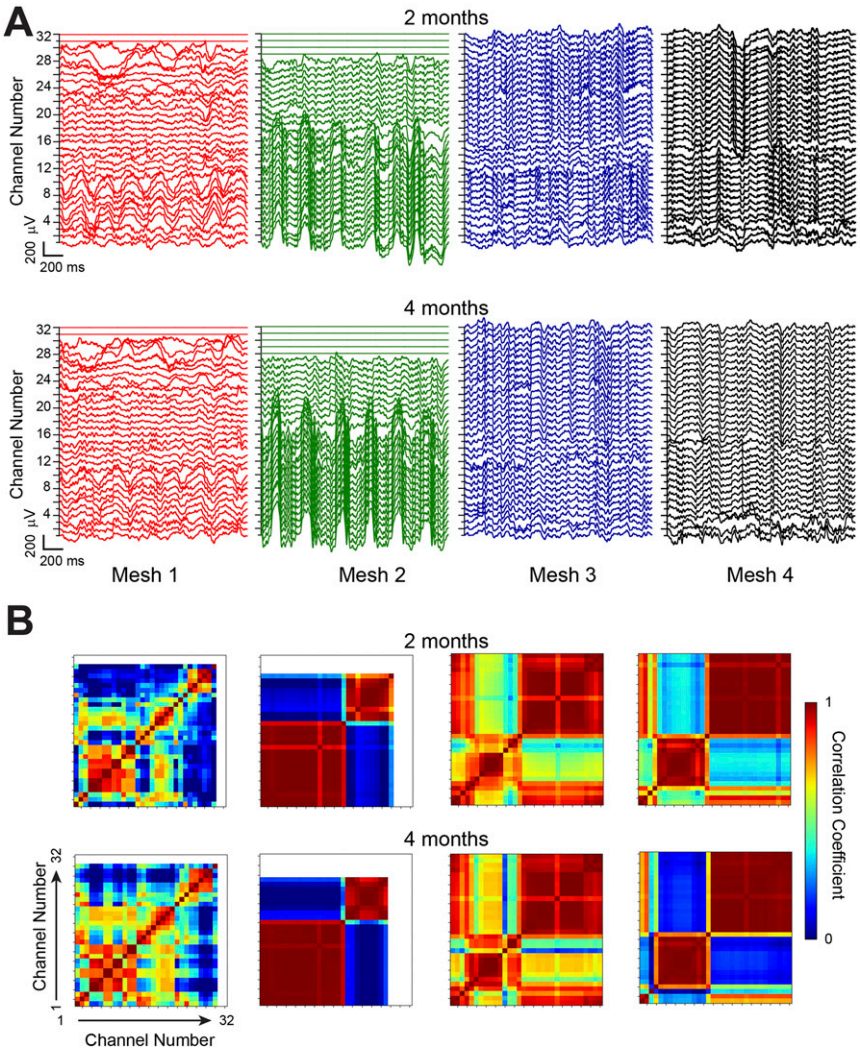

Fig. S2. The 128-channel LFP recording data. (*A*) LFP recordings from the same four 32-channel meshes as shown in Fig. 5*A* at 2 (*Upper*) and 4 (*Lower*) mo postinjection. (*B*) Correlation maps of the 32-channel LFP recordings from each of the four implanted mesh electronics probes at 2 (*Upper*) and 4 (*Lower*) mo postinjection. Colors indicate the correlation coefficient between any two given channels according to the color bar shown on the far right.

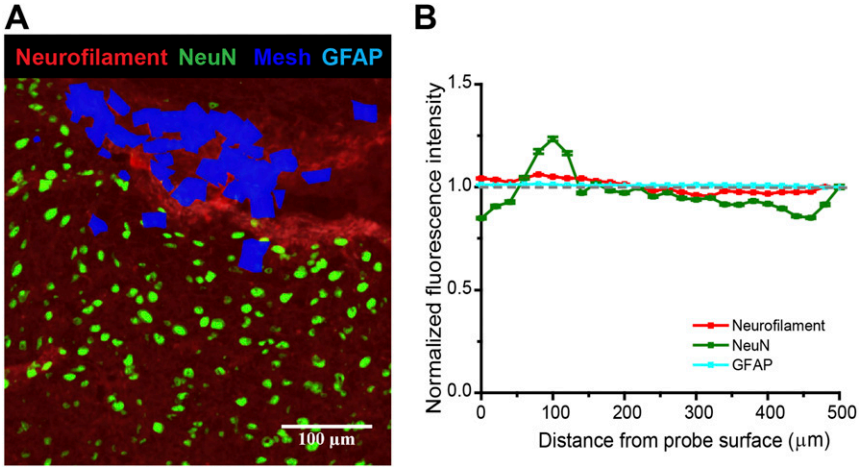

Fig. S3. Histology of horizontal brain tissue slices containing the highly multiplexed mesh electronics 6 wk postimplantation. (*A*) Composite image of an immunostained horizontal hippocampal brain slice implanted with the mesh electronics. The red, green, and cyan colors correspond to neurofilaments, NeuN, and GFAP, respectively, taken by a confocal microscope, and the blue color corresponds to the positions of the mesh electronics elements determined from the DIC image taken by the same microscope with a DIC modality. See *SI Text* for details of extraction of mesh electronics from DIC image. (Scale bar: 100 μm.) (*B*) Neurofilament (red), NeuN (green), and GFAP (cyan) fluorescence intensity normalized against background values (gray dashed horizontal line) plotted versus distance from the mesh electronics interface ($x = 0$). All error bars in this figure reflect ±1 SEM.

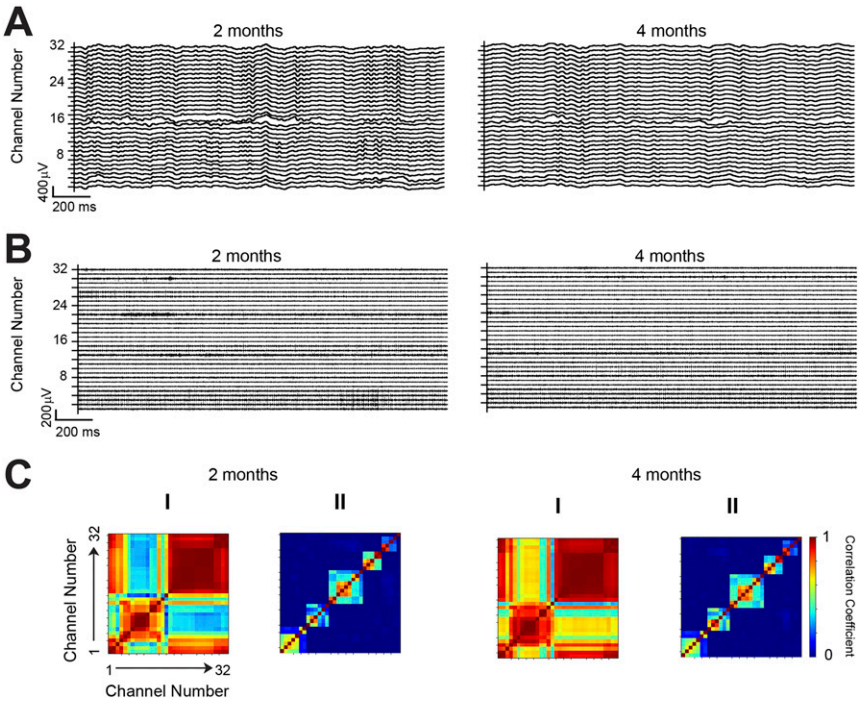

Fig. S4. Representative 32-channel chronic recording data from a freely behaving mouse. (*A*) LFP and (*B*) extracellular spike recordings at 2 (*Left*) and 4 (*Right*) mo postinjection. (*C*) Correlation maps of LFP (*I*) and extracellular spike (*II*) recordings at 2 (*Left*) and 4 (*Right*) mo postinjection. Colors indicate the correlation coefficient between any two given channels according to the color bar shown on the far right. All of the maps were calculated from data shown in Fig. 7*C*. See *Materials and Methods* and *SI Text* for details of correlation coefficient calculations.

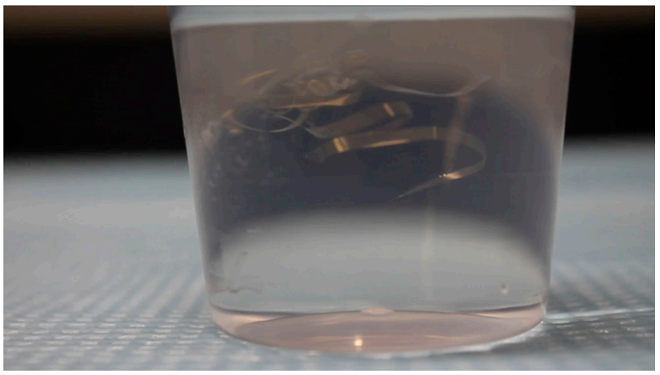

Movie S1. Free-standing 128-channel mesh electronics in aqueous solution. This video shows seven free-standing 128-channel mesh electronics with the design shown in Fig. 1*B*, *III* suspended in water. Manipulation of the mesh electronics using a glass needle demonstrates their robustness of ultraflexibility. The frame rate is 25 frames per second (fps), and the video is played at 1× real time.

Movie S1

Movie S2. Chronic recordings from a freely behaving mouse with implanted 32-channel mesh electronics probe. This video shows a mouse with a head-mounted voltage amplifier roaming freely in a cage with randomly positioned food pellets during recording. The frame rate is 25 fps, and the video is played at 1× real time. The mesh electronics were injected into the hippocampus with electrodes spanning across the hippocampal CA1 and CA3 fields and somatosensory cortex, and connected to PCB and the interface cable as described in *Materials and Methods* and *SI Text*.

Movie S2